VOLUME 4, NUMBER 9, SEPTEMBER 2004

NANO LETTERS

Letters

Coherent Excitation Transport in Metal–Nanoparticle Chains

D. S. Citrin

School of Electrical and Computer Engineering, Georgia Institute of Technology, Atlanta, Georgia 30332-0250

Received February 27, 2004; Revised Manuscript Received July 12, 2004

ABSTRACT

Electromagnetic energy transport in chains of noncontacting metal nanoparticles is studied within an exactly solvable model. The transport is mediated by the retarded electromagnetic interactions between plasmons confined to the individual nanoparticles and therefore self-consistently accounts for spontaneous emission on the same footing as the transport; the propagating hybrid plasmonic-electromagnetic modes of the chain are known as plasmon polaritons. Dark modes are found in the first Brillouin zone when the excitation wavelength is greater than the resonant optical wavelength, suggesting the possibility of the suppression of radiative losses. Nearest-neighbor tight-binding models are shown to be of limited validity.

Recently, there has been great interest in the transport of electromagnetic excitation along chains of noncontacting metal nanoparticles.[1] A plasmon on one nanoparticle in the chain can excite others, resulting in a mobile excitation that can hop down the chain to subsequent nanoparticles due to the retarded dipole−dipole coupling. Nanoparticle chains have attracted interest in part for applications in subwavelength optical guiding structures.[2−6] To facilitate the understanding of experimental data as well as to design structures, simple theoretical models are desired. The bulk of the

10.1021/nl049679l CCC: $27.50
Published on Web 08/04/2004

analyses of excitation transport in these structures to date has been carried out in the framework of the nearest-neighbor tight-binding model (NNTBM).[2−6] The basis for relying on such analyses is the rapid fall off with distance of the dynamic dipole−dipole coupling matrix elements. These have terms that vary as the inverse distance to the first, second, and third powers.[7] Thus, for sufficiently close spacing of the nanoparticles, the matrix elements might be expected to be dominated by the term that varies as inverse distance cubed. It would therefore appear that only the coupling between nearest neighbors need be retained. Finally, since only nearest-neighbor coupling is assumed to be important and the interparticle spacing is much less than the relevant optical wavelength, the nonretarded limit is taken. These assumptions, however, are called into question by the following observations. (i) Direct excitation transfer between distant members of dipolar chains has been predicted in some cases to be important.[8] (ii) The relative roles of the terms in the coupling matrix element differ for longitudinal and transverse excitations (i.e., for dipole moment aligned with or perpendicular to the chain axis). Thus, the lumped effect of the various terms in the NNTBM matrix elements needs to be carefully considered; this has not been carried out. (iii) Spontaneous emission and excitation transport are governed by retarded dipole−dipole coupling. The nonretarded limit, however, neglects radiative losses. Their *ad hoc* reintroduction late in the calculation is likely to be inconsistent. (iv) Attempts to retain retardation effects within a NNTBM can lead to erroneous noncausal results for the radiative decay (apparent negative radiative widths).

These observations raise serious questions about the validity of NNTBMs. In this letter, we show that none of the above approximations need be made at all, and that a single analytically tractable theory can be used to obtain exact model dispersion for the electromagnetic modes in nanoparticle chains. Moreover, the expressions are scalable to different parameters, and thus the results contained in this study are universal. In the following we present a theory of point dipolar excitations coupled by the full retarded dipole−dipole coupling in a linear chain. The theory provides both the real dispersion as well as the radiative width as the position and width of resonances of the dipolar response function of the nanoparticle chain.

The problem is treated as discussed in ref 8 in which long-range dynamic-coupling effects on the transport of exciton polaritons in quantum-dot chains were studied. Our aim is to describe the coupled plasmon-electromagnetic modes, or plasmon polaritons, of a chain of identical spherical and isotropic metal nanoparticles arranged along a line with period d. We neglect substrate-related effects, and the nanoparticles are treated in the point−dipole limit. The plasmon polaritons are given by the poles of the retarded dipole Green function (GF) $D_q(\epsilon)$ (ref 8) where q is the excitation wavevector along the chain and ϵ is the energy. In the site representation, the components of the inverse of $D_q(\epsilon)$ read

$$D^{-1}_{n\alpha,m\beta}(\epsilon) = \frac{\epsilon^2 - \epsilon_p^2}{2\epsilon_p}\delta_{\alpha\beta}\delta_{nm} - i\gamma_{nr}(\epsilon) - \Sigma_{n\alpha,m\beta}(\epsilon) \quad (1)$$

where α and β refer to the directions of the polarization in nanoparticles n and m, respectively, (with $\alpha,\beta = L, T_1, T_2$ denoting polarization in the longitudinal or the two orthogonal transverse directions with respect to the chain axis), m, $n\in\{-\infty, ..., -1, 0, 1, ..., \infty\}$ indexes the nanoparticle site, ϵ_p is the single-nanoparticle plasmon energy, and $\gamma_{nr}(\epsilon) = \mathrm{sign}(\epsilon)\gamma_{nr}$ is the nonradiative contribution to the homogeneous width of the plasmon, which for small nanoparticles ($\sim$20 nm diameter) may be much larger than the radiative width and may thus be the dominant cause of attenuation in the propagation of plasmon polaritons in these structures; larger nanoparticles ($\sim$100 nm) may be primarily radiatively broadened.[9] In particular, $2\gamma_{nr} = 180$ meV was measured for 50 nm Au spherical nanoparticles;[10] $\hbar/2\gamma_{nr}$ of 3.6 fs has been measured in similar nanoparticles.[9,11] The self-energy $\Sigma_{n\alpha,m\beta}(\epsilon)$ contains all radiative effects, including excitation transfer and spontaneous emission,

$$\Sigma_{n\alpha,m\beta}(\epsilon) = \frac{\kappa^2}{\epsilon_b}\int d^3r_1 \int d^3r_2\, \mathbf{p}_{n\alpha}(\mathbf{r}_1)[\overleftrightarrow{T} r^{-1} e^{i\kappa r}]\mathbf{p}_{m\beta}(\mathbf{r}_2) \quad (2)$$

with $\mathbf{p}_{n\alpha}(\mathbf{r}_1)$ the polarization density associated with the plasmon dipole moment on nanoparticle n in direction α, $r = |\mathbf{r}_1 - \mathbf{r}_2|$, $\kappa = \epsilon\sqrt{\epsilon_b}/\hbar c$, $\overleftrightarrow{T} = -\overleftrightarrow{1} - \kappa^{-2}\nabla\nabla$, ϵ_b the background dielectric constant near ϵ_p, and c the in vacuo speed of light.[8] The following identity[7] can be used to simplify eq 2:

$$\kappa^2 \overleftrightarrow{T}\frac{1}{r}e^{i\kappa r} = -\kappa^2(\overleftrightarrow{1} - \hat{\mathbf{r}}\hat{\mathbf{r}})\frac{1}{r}e^{i\kappa r} + (1 - i\kappa r)(\overleftrightarrow{1} - 3\hat{\mathbf{r}}\hat{\mathbf{r}})\frac{1}{r^3}e^{i\kappa r} + \frac{4\pi}{3}\delta^3(\mathbf{r}) \quad (3)$$

Because of the discrete translational symmetry along the chain axis, the modes are diagonal in the excitation wavevector q. In addition, the L-, T_1-, and T_2-modes are all uncoupled (orthogonal) and the two transverse modes degenerate (neglecting substrate effects). We will denote them henceforth as T without a subscript. We thus have

$$D^{-1}_{q,\alpha\beta}(\epsilon) = \sum_{j=-\infty}^{\infty} D^{-1}_{j,\alpha\beta}(\epsilon)e^{-2\pi i q j d}\delta_{\alpha,\beta} \quad (4)$$

where $j = n - m$. Here and below, we incorporate real single-nanoparticle radiative renormalizations into the value of ϵ_p.

To obtain results that can be scaled to any value of the dipole moment, it is useful to calculate the self-energies normalized by a parameter associated with the single-nanoparticle radiative width $2\gamma/3$ (ref 12) with

$$\gamma = \frac{\kappa^3}{\epsilon_b}\left|\int d^3r\, \mathbf{p}(\mathbf{r})\right|^2 \quad (5)$$

Moreover, we define $k = qd$ and $\chi = \kappa d$; χ is the product of the optical wavevector in the background dielectric medium and the period and is therefore a dimensionless measure of the *optical* wavevector, while k is the dimensionless *excitation* wavevector. We finally normalize the self-energy to γ as $\sigma_{k,\alpha}(\chi) = \Sigma_{q,\alpha}(\epsilon)/\gamma$, which is the quantity plotted throughout. Using the foregoing expressions, the normalized self-

energies for the T and L modes are straightforwardly calculated as

$$\sigma_{k,T}(\chi) = -\frac{2}{3}i + \beta_1(k,\chi) + \beta_2(k,\chi) \tag{6}$$

$$\sigma_{k,L}(\chi) = -\frac{2}{3}i - 2\beta_1(k,\chi) \tag{7}$$

where

$$\beta_1(k,\chi) = \sum_{j=-\infty}^{\infty}{}' \left(\frac{1}{\chi^3|j|^3} - \frac{i}{\chi^2 j^2}\right) e^{ikj} e^{i\chi|j|} \tag{8}$$

$$\beta_2(k,\chi) = \sum_{j=-\infty}^{\infty}{}' \frac{1}{\chi|j|} e^{ikj} e^{i\chi|j|} \tag{9}$$

$$= \frac{1}{\chi}\log[2e^{i\chi}(\cos\chi - \cos k)] \tag{10}$$

$\sum_{j=-\infty}^{\infty}{}'$ excludes the term for $j = 0$.

The response function $D_{q,\alpha}(\epsilon)$ contains all the physical information about the system. For example, the modes can be defined as the zeros of $D_{q,\alpha}^{-1}(\epsilon) = (\epsilon^2 - \epsilon_p{}^2/2\epsilon_p) - i\gamma_{nr}(\epsilon) - \Sigma_{q,\alpha}(\epsilon)$, i.e., the dispersion relation is $D_{q,\alpha}^{-1}(\epsilon) = 0$. Another useful quantity in the spectral density is $-2\mathrm{Im}\, D_{q,\alpha}(\epsilon)$, which is proportional to the density of states. Its peak positions give the mode frequencies and the widths as the inverse of the radiative lifetimes of the resonances. Although a full analysis of the response function is easily carried out now that we have explicit expressions for the self-energy, a simple pole approximation is frequently useful to elucidate the physical origin of features in the mode spectrum. Namely, if $|\Sigma_{q,\alpha}(\epsilon)| \ll \epsilon_p$, then to a good approximation the complex energy $\epsilon_{q,\alpha}$ of the mode can be obtained by the pole and resonance approximations $\epsilon_{q,\alpha} = \epsilon_p - i\gamma_{nr} + \Sigma_{q,\alpha}(\epsilon_p)$, the real part giving the position of the resonance and the imaginary part its width.

In Figure 1 are shown in the first column Re $\sigma_{k,T}(\chi)$ and $-\mathrm{Im}\, \sigma_{k,T}(\chi)$ as functions of χ and k, while in the second column are shown Re $\sigma_{k,L}(\chi)$ and $-\mathrm{Im}\, \sigma_{k,L}(\chi)$. Figure 2 shows horizontal cuts at $\chi = 0.1$ to assist in the visualization of the scale (solid curves). For $\chi \to 0$, the dispersion for the T-mode starts at small normalized wavevector k at a maximum (light) and progresses to a minimum at the Brillouin zone boundary at $k = \pi$ (dark). This is the expected behavior for a transverse mode.[13] By contrast, for small χ the L-mode has a maximum at $k = 0$ and reaches a maximum at $k = \pi$—the behavior characteristic of a longitudinal mode (cf. Figure 1 of ref 14). For both the T- and the L-modes, $-\mathrm{Im}\, \sigma_{k,\alpha}(\chi) = 0$ for $\chi < k$ (or $\kappa < q$ or $\lambda_{optical} > \lambda_{excitation}$). This means that radiative decay is suppressed in this region of parameter space. In other words, there is no density of propagating electromagnetic modes in $\chi < k$ into which the excitation can decay.[14−18] Each time the zone-folded $\chi = k$ line (light line) is crossed, new far-field propagating electromagnetic modes are accessed for radiative decay. This effect is particularly pronounced for the T-mode due to the logarithmic term of eq 10, which leads to a step function in $-\mathrm{Im}\, \sigma_{k,T}(\chi)$. A highly radiative region is seen at small

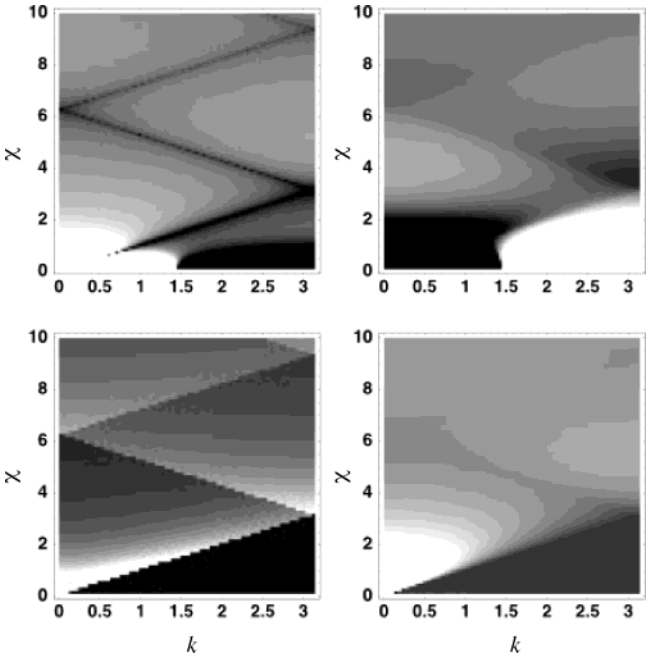

Figure 1. Re $\sigma_{k,\alpha}(\chi)$ (upper row) and $-\mathrm{Im}\, \sigma_{k,\alpha}(\chi)$ (lower row) for the $\alpha = T$-mode (left column) and the $\alpha = L$-mode (right column) plotted as functions of dimensionless excitation wavevector k and dimensionless frequency χ.

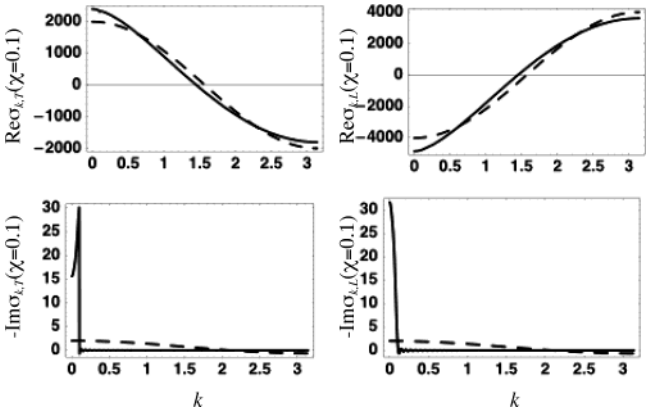

Figure 2. Re $\sigma_{k,\alpha}(\chi)$ (upper row) and $-\mathrm{Im}\, \sigma_{k,\alpha}(\chi)$ (lower row) for the $\alpha = T$-mode (left column) and the $\alpha = L$-mode (right column) as in Figure 1, but plotted as functions of dimensionless excitation wavevector k for $\chi = 0.1$ (solid curves). Dashed curves show results within the nearest-neighbor tight-binding model.

wavevector and energy with $\chi > q$ just above the light line. This appears as the peak near $k = 0$ in the solid curves in the lower frames of Figure 2.

We reiterate that the curves of Figure 1 (eqs 6 and 7) are universal in that they can be scaled for any value of the parameters γ and d.

At this stage we make a comparison with the comparable curves obtained by truncating the summations at the $j = \pm 1$ terms in eq 8. Figure 3 shows results similar to those in Figure 1, but calculated for the NNTBM. Overall, the results for Re $\sigma_{k,\alpha}(\chi)$ are quite poorly approximated by the NNTBM, although they are similar to the exact results for $\chi \to 0$. This is seen in more detail in Figure 2, which shows a comparison of Re $\sigma_{k,\alpha}(\chi)$ calculated with all neighbors compared to what is obtained if only the nearest neighbors are retained for χ

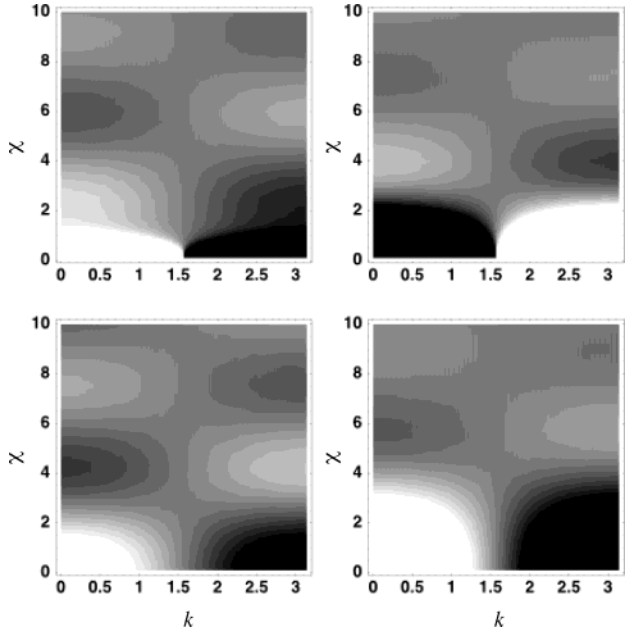

Figure 3. Re $\sigma_{k,\alpha}(\chi)$ (upper row) and $-$Im $\sigma_{k,\alpha}(\chi)$ (lower row) for the $\alpha = T$-mode (left column) and the $\alpha = L$-mode (right column) calculated within the nearest-neighbor tight-binding model plotted as functions of dimensionless excitation wavevector k and dimensionless frequency χ.

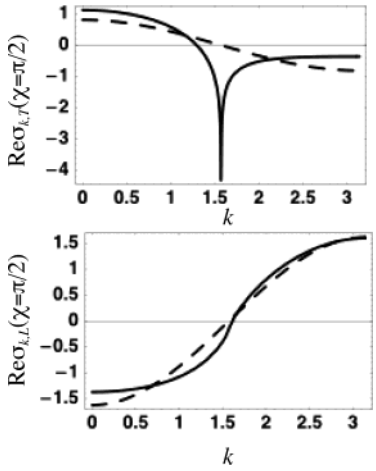

Figure 4. Re $\sigma_{k,\alpha}(\chi)$ for the $\alpha = T$-mode (upper frame) and the $\alpha = L$-mode (lower frame) as in Figure 1, but plotted as functions of dimensionless excitation wavevector k for $\chi = \pi/2$ (solid curves). Dashed curves show results within the NNTBM.

$= 0.1$. The real dispersion is thus well approximated by the NNTBM in this regime. Referring again to Figure 2, the NNTBM is observed to be an entirely inadequate approximation to the dispersion in the radiative width, and moreover produces spurious negative results. This is because the radiative width is determined by the interference of the radiation arising from all the nanoparticles, and is thus a global property of the structure.

In Figure 4 is shown Re $\sigma_{k,\alpha}(\chi)$ for $\chi = \pi/2$. In this case, the NNTBM is seen to be a particularly poor approximation, especially for the T-mode which contains a logarithmic divergence at the light line (here $k = \chi = \pi/2$).

One might expect that the effective range of the interaction would be given by the attenuation length for propagation. In refs 9−11, dephasing rates of several fs were measured for ∼20 nm Au nanoparticles. This is consistent with ∼10 nm attenuation lengths observed in ref 6, taking the maximum group velocity from the dispersion obtained in a NNTBM. As we now argue, the attenuation length for plasmon polaritons is not directly relevant to the range of the interparticle interaction. Consider eq 3 which gives the interparticle coupling. Any exponential cutoff to the range of this coupling will enter in the exponential factors $\exp(i\kappa|\, n - n|\, d)$ provided κ has an imaginary part. Recall $\kappa = \epsilon\sqrt{\epsilon_b}/(\hbar c)$. Thus, to address the question of finite range, we should modify our pole approximation such that ϵ is replaced by $\epsilon_p - i\gamma_{nr}$, where we assume quite reasonably that the dephasing is dominated by nonradiative processes. Then, effectively, the self-energy would contain the factor $\exp(-i\gamma_{nr}|\, m - n|\, d\sqrt{\epsilon_b}/(\hbar c))$. This would imply a range of $\hbar c/(\gamma_{nr}\sqrt{\epsilon_b})$. Assuming a center frequency in the optical regime and γ_{nr} on the order of 10% the center frequency, we obtain an interparticle-coupling range of $\sim 1-10$ μm, which is much greater than typical attenuation lengths. From this we can conclude that long-range coupling plays a significant role even in the presence of significant attenuation.

It is instructive to explore the effective masses $m^*_{k,T}(\chi)$ and $m^*_{k,L}(\chi)$ of the modes. We have

$$\frac{1}{m^*_{k,\alpha}(\chi)} = \frac{\gamma d^2}{\hbar^2}\frac{\partial^2}{\partial k^2}\sigma_{k,\alpha}(\chi) \tag{11}$$

Using eqs 10 and 9, this can be expressed in terms of

$$\frac{\partial^2\beta_1(k,\chi)}{\partial k} = -\frac{1}{\chi^2}\left\{\beta_2(k,\chi) + \frac{1}{2}\left[e^{i(\chi+k)/2}\csc\frac{\chi+k}{2} + e^{i(\chi-k)/2}\csc\frac{\chi-k}{2}\right]\right\} \tag{12}$$

$$\frac{\partial^2\beta_2(k,\chi)}{\partial k} = \frac{1}{\chi}\frac{\cos k\cos\chi - 1}{(\cos\chi - \cos k)^2} \tag{13}$$

Figure 5 shows the real parts of the scaled effective masses Re $[\partial^2\sigma_{k,\alpha}(\chi)/\partial k^2]^{-1}$ for the T- and L-modes. Near the light line for the T-mode, the nonanalytic behavior of the dispersion may prevent one from simply attributing Re $[\partial^2\sigma_{k,T}(\chi)/\partial k^2]^{-1}$ to m^*_T. The imaginary part of the effective masses can be interpreted of as motion-induced attenuation via radiative decay of the plasmon polariton. For small χ, $q \to 0$, $m^*_T < 0$, while $m^*_L > 0$, as might be expected from the curvature of the dispersion.

A number of the effects found here were anticipated by earlier work on exciton polaritons in semiconductor quantum wires,[14,15,17,18] where the logarithmic dependence of the self-energy on k and χ (essentially in the limit $d \to 0$) and the quenching of the logarithmic singularity at $\chi = k$ for the longitudinal mode were found.

To conclude, we have presented easily implemented, exact numerical calculations of the plasmon polariton modes in chains of noncontacting metal nanoparticles assuming point dipoles coupled via the retarded dipole−dipole interaction. The calculations describe radiative decay on the same footing

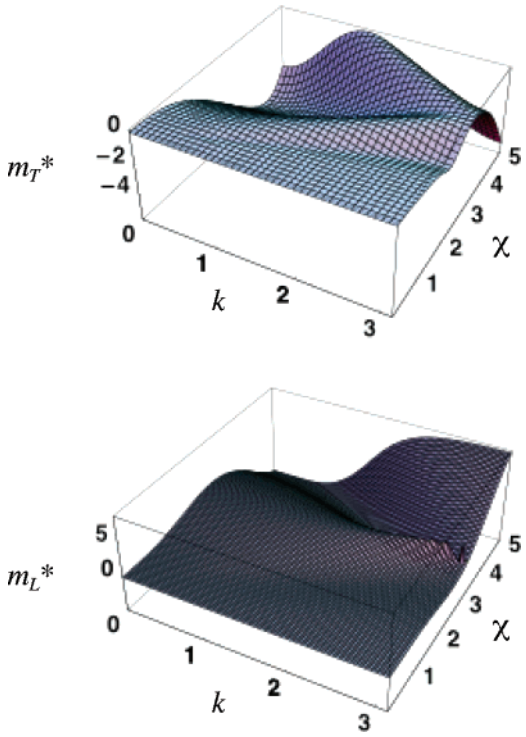

Figure 5. The real part of the scaled effective masses m_α^* for the $\alpha = T$-mode (upper frame) and the $\alpha = L$-mode (lower frame) [right-hand side of eqs 12 and 13]. Note that the scale of the χ axis is half that in Figures 1 and 3.

as the excitation transport. Dark modes are found in the first Brillouin zone for $\chi < k$, suggesting the possibility of suppressing radiative losses in nanoplasmonic waveguides. In particular, noble-metal nanoparticle chains with particle diameters in the 100 nm range might sustain low-attenuation propagation via dark modes which can potentially be excited using near-field techniques. The NNTBM is found to provide a reasonable description of the real mode dispersion in the long-wavelength limit $\chi \ll k$, but found to fail when this condition is not satisfied. We have also elucidated the role of long-range coupling, even in the presence of severe attenuation. Moreover, the imaginary part of the dispersion, giving the radiative width, cannot be calculated adequately at all in the NNTBM, as it results in spurious negative radiative widths as well as the possibility of radiative decay of modes known to be dark.

Acknowledgment. The author thanks S. E. Ralph for helpful discussions. This work was supported in part by the National Science Foundation through grant NSF-DMR-0303969.

References

(1) Quinten, M.; Leitner, A.; Kren, J. R.; Aussenegg, F. R. *Opt. Lett.* **1998**, *23*, 1331.
(2) Maier, S. A.; Brongersma, M. L.; Kik, P. G.; Meltzer, S.; Requicha, A. A. G.; Atwater, H. A. *Adv. Mater.* **2001**, *13*, 1501.
(3) Maier, S. A.; Brongersma, M. L.; Atwater, H. A. *Mater. Res. Soc. Symp. Proc.* **2001**, *637*, E2.9.1.
(4) Maier, S. A.; Kik, P. G.; Atwater, H. A. *Appl. Phys. Lett.* **2002**, *81*, 1714.
(5) Maier, S. A.; Brongersma, M. L.; Atwater, H. A. *Appl. Phys. Lett.* **2001**, *78*, 16.
(6) Maier, S. A.; Brongersma, M. L.; Kik, P. G.; Atwater, H. A. *Phys. Rev. B* **2002**, *65*, 193408.
(7) Avery, J. S. *Proc. Phys. Soc.* **1966**, *88*, 1.
(8) Citrin, D. S. *Opt. Lett.* **1995**, *20*, 901.
(9) Sönnichsen, C.; Franzl, T.; Wilk, T.; von Plessen, G.; Feldmann, J.; Wilson, O.; Mulvaney, P. *Phys. Rev. Lett.* **2002**, *88*, 77402.
(10) Maier, S. A.; Kik, P. G.; Atwater, H. A.; Meltzer, S.; Requincha, A. A. G.; Koel, B. E. *Proc. SPIE* **2002**, *4810*, in press.
(11) Klar, T.; Perner, M.; Grosse, S.; von Plessen, G.; Spirkl, W.; Feldmann, J. *Phys. Rev. Lett.* **1998**, *80*, 4249.
(12) This corrects a minor error in ref 8.
(13) Brongersma, M. L.; Hartman, J. W.; Atwater, H. A. *Phys. Rev. B* **2002**, *62*, R16356.
(14) Citrin, D. S. *Phys. Rev. B* **1993**, *48*, 2535.
(15) Citrin, D. S. *Phys. Rev. Lett.* **1992**, *69*, 3393.
(16) Agranovich, V. M.; Dubovskii, O. A. *Pis'ma Zh. Eksp. Teor. Fiz.* **1966**, *3*, 345 [*JETP Lett.* **1966**, *3*, 223].
(17) Tassone, F.; Bassani, F. *Nuovo Cimento* **1992**, *14D*, 1241.
(18) Jorda, S. *Solid State Commun.* **1993**, *87*, 439.

NL049679L